Title

Practical microcircuits for handheld acoustofluidics

Journal

Lab on a Chip, 21(7)

ISSN

1473-0197

Authors

Huang, An

Connacher, William

Stambaugh, Mark

et al.

Publication Date

2021-04-07

DOI

10.1039/d0lc01008a

Peer reviewed

Journal Name

ARTICLE TYPE

Cite this: DOI: 00.0000/xxxxxxxxxx

Practical Microcircuits for Handheld Acoustofluidics †

An Huang,[‡a,b] William Connacher,[‡a,b] Mark Stambaugh,[c] Naiqing Zhang,[b] Shuai Zhang,[a,b] Jiyang Mei,[a,b] Aditi Jain,[c] Sravya Alluri,[c] Vincent Leung,[c,d] Anushi E Rajapaksa,[e] and James Friend[*a,b]

Received Date
Accepted Date

DOI: 00.0000/xxxxxxxxxx

Acoustofluidics has promised to enable lab-on-a-chip and point-of-care devices in ways difficult to achieve using other methods. Piezoelectric ultrasonic transducers—as small as the chips they actuate—provide rapid fluid and suspended object transport. Acoustofluidic lab-on-chip devices offer a vast range of benefits in early disease identification and noninvasive drug delivery. However, their potential has long been undermined by the need for benchtop or rack-mount electronics. The piezoelectric ultrasonic transducers within require these equipment and thus acoustofluidic device implementation in a bedside setting has been limited. Here we detail a general process to enable the reader to produce battery or mains-powered microcircuits ideal for driving 1–300 MHz acoustic devices. We include the general design strategy for the circuit, the blocks that collectively define it, and suitable, specific choices for components to produce these blocks. We furthermore illustrate how to incorporate automated resonance finding and tracking, sensing and feedback, and built-in adjustability to accommodate devices' vastly different operating frequencies and powers in a single driver, including examples of fluid and particle manipulation typical of the needs in our discipline. With this in hand, the many groups active in lab-on-a-chip acoustofluidics can now finally deliver on the promise of handheld, point-of-care technologies.

1 Introduction

The challenge to deliver a miniaturized solution to driving acoustofluidics devices has eluded the research community for over twenty-five years. The knowledge and know-how required to design MHz-frequency, high-power driver circuits in a small package is surprisingly rare among the many advancements in microelectronics technologies over the past seventy-five years, and is constraining progress in research and development of acoustofluidics as a potential method for delivering effective lab-on-a-chip devices into commercial and clinical use. The original use of surface acoustic wave (SAW) devices in microfluidics[1] resulted in the formation of a company, Advalytix AG, eventually owned by Becton & Dickinson focused on SAW-driven fluid mixing at small scales, yet the drivers for this commercial product were both mains powered and large. Other, occasional reports of success have been claimed, only to learn that the circuit fails after only a short time[2], or that power wires were hidden in a shirt sleeve for a "handheld" driver. Several attempts to completely avoid the problem of MHz-order acoustofluifdics have been attempted with lower frequency devices and corresponding driver circuits. Bachman *et al.*[3] produced an acoustofluidic system based on a cell phone and an audio speaker, but this scheme is limited to <30 kHz. They also developed a system based on an Arduino and a motor controller, but this only increased the upper frequency limit to 65 kHz[4]. While useful, the long wavelengths of these low frequency devices are not suitable for microfluidics that define most lab-on-a-chip technologies, and there is the potential for cell and molecular damage from such low frequency acoustics. While some may contend that the "pull" for acoustofluidics as a technology sufficient to justify investment in developing circuits and other technologies to make it practical in applications, we suggest that overcoming some of the risk and enabling broader

[a] *Materials Science and Engineering Program, University of California San Diego, 9500 Gilman Drive, La Jolla, CA 92093 USA.*
[b] *Medically Advanced Devices Laboratory, Center for Medical Devices, Department of Mechanical and Aerospace Engineering, Jacobs School of Engineering, and the Department of Medicine, School of Medicine, University of California San Diego, 9500 Gilman Drive MC0411, La Jolla, CA 92093 USA.*
[c] *Qualcomm Institute, University of California San Diego, 9500 Gilman Drive, University of California San Diego, 9500 Gilman Drive, La Jolla, CA 92093 USA.*
[d] *Now Associate Professor, Electrical Engineering Department, Baylor University, Waco, TX 76798–7141*
[e] *New Vaccines, Murdoch Children's Research Institute, Parkville, Victoria 3052 Australia; Neonatal Research, Royal Children's Hospital, Parkville, VIC, Australia; Newborn Research, Royal Women's Hospital, Parkville, VIC, Australia; Department of Paediatrics, University of Melbourne, Parkville, VIC, Australia.*
∗ *Corresponding author. Web:* `http://friend.ucsd.edu`*; E-mail: jfriend@ucsd.edu*
‡ *These authors contributed equally to this work.*
† Electronic Supplementary Information (ESI) available: Video illustrating use of TM and SAW circuit boards in typical acoustofluidics applications. See DOI: 10.1039/cXCP00000x/

testing and adoption of acoustofluidics can only help its maturation into a beneficial technology.

This paper aims to provide the first comprehensive microcircuit design capable of reliably driving the vast majority of acoustofluidics devices at 1–300 MHz, including the strategy and details necessary to help the reader to build their own driver circuits for lab-on-a-chip acoustofluidics.

Acoustofluidic devices are ideally suited for point-of-care and lab-on-a-chip applications, as they are small and produce ample mechanical power that can be harnessed to transport fluids and suspended objects. When alternating current (AC) signals are applied to piezoelectric transducers used in these devices, the resulting acoustic waves produce direct forces at boundaries with acoustic impedance changes and acoustic streaming from the attenuation of the acoustic wave in the fluid and within the viscous boundary layer. In doing so, acoustofluidics offers the following advantages over other approaches: (i) the forces formed from high frequency acoustic waves overcome surface and viscous-mediated forces that tend to dominate in microfluidics, (ii) acoustic waves enable label-free, non-contact particle manipulation at small scales, and (iii) the AC signals that directly drive these devices offer precise control and simple operation. Fluid mixing, droplet manipulation, particle manipulation, and atomization have all been demonstrated with acoustofluidic technology and helped overcome medical and diagnostic challenges[5–7]. However, the majority of these solutions have not found practical use because they are unable to be adapted to miniature, portable devices. They still require laboratory equipment including signal generators, amplifiers, and oscilloscopes.

Many point-of-care devices and all drug delivery and disease evaluation technologies must also avoid damaging biological samples. The absence of damage to biological molecules and cells has been shown repeatedly in high frequency acoustic devices[8–10], but lower frequency acoustic waves, on the order of 10 kHz, are known to cause cavitation[11] that can damage cells, proteins, and antibodies, even—for example—in modulating higher frequency acoustics devices[2].

To highlight the capabilities of our circuit design for enabling lab-on-a-chip concepts and work, we will demonstrate four acoustofluidics devices that utilize our microcircuit. We will first demonstrate quick mixing in a sessile drop using a surface acoustic wave (SAW) device driven by our microcircuit. The Reynolds number, $\mathrm{Re} = \rho u D/\mu$, must be large for the turbulent flow that characterizes mixing, and it scales with the length scale of the device, D, so that it is very difficult to generate mixing at the microscale. The earliest broadly known lab-on-a-chip application of SAW devices solved precisely this problem[12]. Very high frequency acoustic waves transmitted into fluids in contact with these SAW devices lead to large accelerations that easily mix a broad range of fluids from glycerol to whole blood[13–15].

We next demonstrate tunable alignment of 2 μm particles with SAW of 40–80 MHz, another key application of acoustofluidics in lab-on-a-chip applications. The spacing between groupings of particles aligned using standing waves is determined by their frequency[16]. Furthermore, The ability to manipulate small particles with acoustic transducers[17] depends on the wavelength of the acoustic waves they generate.

Similarly, the isolation and manipulation of medically relevant particles—cells, organelles, biomolecules—with acoustofluidic devices[18] requires frequencies beyond 10 MHz. We demonstrate separation of 38 μm and 4 μm diameter particles in a sessile drop as an analog to blood sample separation.

These three SAW based applications are each demonstrated using the same handheld driver circuit, named the *SAW board*, reprogrammed for each case by quickly uploading code from a computer. This board is relatively large—the size of an open hand—and is plugged in to wall power, convenient for prototyping, testing, and saving data.

In the fourth case, we demonstrate a high power application, a nebulizer driven by a handheld, battery powered circuit. This circuit, named the *TM* (thickness mode) *board* is designed using the same principles, but is optimized in parts and layout to be a compact, near-commercial circuit design. Nebulization is accomplished at practically relevant flow rates from battery power using this circuit and the board comes pre-loaded with a program to run a simple user interface. Acoustofluidic atomization of therapeutic liquids has the potential to replace other forms of nebulization because of the aforementioned biological compatibility and the proven ability to produce droplet sizes in the range for optimal delivery to the lungs[19–21]. Our circuit enables these benefits in a handheld device.

2 Circuit design for acoustofluidics

To suit the signal generation needs of acoustofluidics devices while offering the portability required in clinical and commercial applications, a driver circuit must be miniaturized, battery powered, and able to produce signals in the 1–300 MHz frequency range with a power of 50 mW to 2 W, based upon most of the past published work in this discipline[7,22–24].

Benchtop equipment—signal generators, DC power supplies, and low-frequency (LF) to radio-frequency (RF) amplifiers—is simply too expensive, bulky, and heavy for use outside of research laboratories. Miniaturized electronics tailored to an application may be achieved using commercially available *off-the-shelf* electronic parts assembled on custom-designed printed circuit boards (PCB). Because of the unique power and frequency requirements of acoustofluidics devices, significant design, programming, and testing efforts are required, but nonetheless can produce compact and user-friendly devices.

We accomplish this by applying electronics design principles to develop two distinct driving circuits, the TM board for 1–25 MHz thickness mode (TM) transducers, and the SAW board for 30–100 MHz SAW transducers. The TM board is compact, as it is intended for battery-driven handheld nebulization. The SAW board was originally developed to drive SAW within prototype lithium batteries[25] on the lab benchtop. Consequently, the SAW board is larger for convenience, requires less power, operates at a higher frequency range, and draws power from a wall outlet. It also has additional circuitry on the board used for charging and other purposes not relevant to the work reported in this paper. Here, we use the TM board to illustrate how the reader may make practical handheld driver circuits for acoustofluidics sufficient to

even drive atomization. Both designs, with minor modifications, may be used for driving acoustofluidic devices from a few kHz to 250 MHz or more. We use the SAW board to demonstrate three other acoustofluidic applications showcasing the adaptability of this circuit design. With some effort, the reader should be able to construct a prototype circuit such as the SAW board for their needs, and once a specific application is identified, a much smaller prototype driver like the TM board may then be produced.

2.1 Circuit blocks

Despite the differences in the required stimulus frequencies and power levels, electrical driver systems for acoustofluidic devices incorporate five basic units or *blocks*.

1. **Stimulus generation**: This is accomplished by semiconductor circuits known as *phase locked loops* (PLL), a type of frequency synthesizer. This low-cost solution uses a reference crystal oscillator to produce a highly accurate and stable tone. The frequency is programmable over a specified range with very fine resolution, in this case <0.01 MHz. However, unlike the benchtop signal generators or arbitrary waveform generators (AWG) it replaces, the output amplitude is usually fixed; PLLs typically cannot produce the required output power to directly drive the SAW devices. This leads us to the next circuit block.

2. **Amplification**: We employ a chain of amplifiers to connect the output of the PLL to the input of the SAW device, achieving increasingly higher voltage swings as needed. Furthermore, duty cycle control can be added using the enable signals of clock buffers, while attenuators—using dedicated chips or a simple resistor voltage divider—can be used to fine-tune the signal swing, and a power amplifier with a push-pull output stage can be employed to efficiently deliver high current at fixed voltage to the device. The device itself can be modeled as a low impedance load at the resonance frequency.

3. **Power management**: From a single battery or a wall outlet, the power management unit (PMU) produces all voltage supplies (such as 3.3V, 5V, 24V etc.) as required by various semiconductor chips on the PCB. These circuits are commonly known as *DC-DC converters*. *Boost converters* are used to step-up voltages from input to output, while *low dropout* (LDO) regulators step-down voltages. If higher efficiency is required, a step-down function can also be achieved using a *buck converter*. This block replaces a typical benchtop power supply.

4. **Impedance matching**: In a typical bench-top setup, maximum power transfer is achieved when the load and source impedances match. Signal generators, amplifiers, and cables are typically matched to have 50Ω impedance, for example. If there is an impedance mismatch between two components, some fraction of the power is reflected at the impedance interface. Based on a simple source/load model, the power dissipated by the load is $P_l = V_s^2 R_l/(R_s + R_l)^2$. However, our boards utilize a constant voltage operational amplifier, so there is no defined source impedance with which to match the load impedance. In this case, power transfer, $P_l = V_s^2/Z_r$, is maximized by minimizing the load impedance, $Z_l = Z_r + iZ_i$, where the real impedance, Z_r, is resistance and the imaginary impedance, Z_i, is capacitive if positive and inductive if negative. At a resonance frequency, $Z_i = 0$ by definition, and we can minimize Z_r by choosing the resonance frequency with the smallest resistance (this is done automatically on our boards as will be explained in the next section). Design choices for the piezoelectric device can aid the reduction in resistance, for example, ensuring the metal electrodes are sufficiently thick whether it is a SAW, flexural, thickness, or some other type of device.

   An impedance matching network is effective at reducing the reflected power in a standard bench-top setup or in a circuit with a source impedance. Such networks do impose a power loss, so the system must be optimized to account for this trade-off. Qualitative examples and additional tips on electrical design are provided by Winkler et al., who show that impedance matching networks can result in a 30% improvement in acoustic performance (in terms of streaming velocity)[26]. In contrast, the power to the transducer in our circuit could be increased by lowering the effective load resistance. Our boards have designated spots for an impedance network, but they have not been populated because the power transfer was already sufficient for demonstration purposes.

   In commercial acoustofluidic products, it will be necessary to measure the impedance of the transducer in the condition it will be used, i.e., within the driver circuit and with realistic mechanical loading with fluids, mounting, wicking, and other attachments. The impedance matching network would be defined from these conditions at the intended frequency. For a transducer used at only one frequency, the simple network designed into our boards or an inductor/capacitor impedance matching network in the case of a more typical set-up is sufficient. Kim et al. utilized an impedance matching network and showed that it leads to more efficient production of acoustic pulses for cell actuation[27]. For multi-frequency applications, more complicated networks are required. Vivek Rathod has covered these and other related topics at length in a recent review[28].

5. **Control and user interface**: A micro-controller unit (MCU), such as the *Arduino Nano* (Arduino LLC, Boston, MA USA), serves as the interface between the electronic driver system and the user. Through general-purpose integrated circuit (I^2C) input-output (IO) expanders, the MCU translates user inputs into low-level digital signals to control all components on the PCB. The MCU can be connected via USB to a laptop for convenient programming and testing flexibility. It may also be pre-programmed with a few options—such as power on/off, frequency up/down—that are selected by onboard push buttons connected to the MCU. As a result, the final SAW-based system may be turned into a completely self-contained and user-friendly device.

6. **Sensing and feedback**: While the electronics described above are already sufficient to drive the SAW device, we can take advantage of modern electronics to offer additional features. For example, one can include thermistors to monitor the board temperature in strategic locations to detect overheating or out-of-design operation. Digitized and read by the MCU, the measured data can be used to simply monitor the operating conditions or to act on the data via a feedback loop, for example, to automatically shut down when a component overheats. As will be discussed below, our systems incorporate current sensors on the SAW device inputs to automatically seek the optimal resonance frequency despite inevitable resonance frequency variations during operation and between devices.

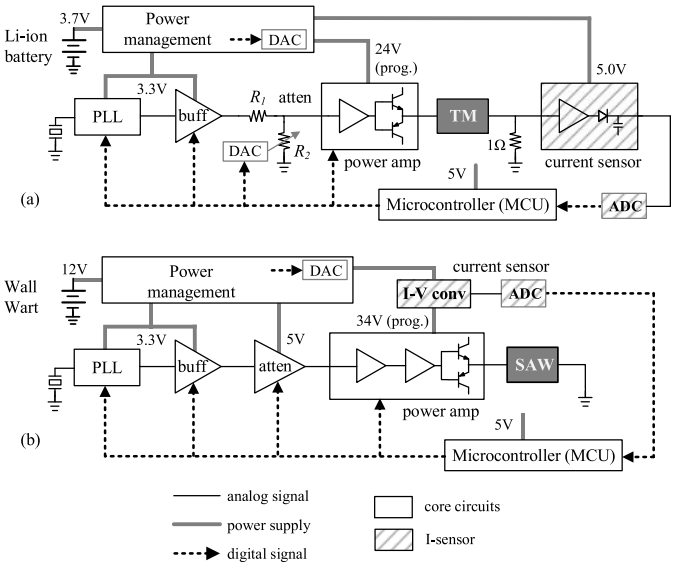

Fig. 1 Block diagrams of the driving circuits. The (a) TM board is designed to drive a 1–25 MHz thickness mode (TM) transducer in a handheld, battery-powered nebulizer, and the (b) SAW board, designed to drive a 30–100 MHz SAW transducer, originally for enhancing the capacity of a rechargeable lithium metal battery, but useful for a broader range of acoustofluidics applications as illustrated later.

The TM and SAW boards embody these principles. Their block diagrams are shown in Fig. 1, and we will explain their specific implementations, including design choices, parts, layout, testing, and a step-by-step guide in later sections.

2.2 Automatic resonance search

In addition to the circuit blocks discussed in the last section that are required for basic functionality, both systems also include blocks to perform a resonance search. The PLL frequency range is swept by the MCU with a frequency step of 1 kHz, and the output current to the SAW device is measured, digitized, and recorded at each frequency step. An initial search range is specified in the algorithm to both minimize the time required to perform the sweep and reduce the risk of a spurious resonance mode's selection. The voltage amplitude, V, at the final stage of the signal chain and in the driver amplifier, is constant by virtue of its resistor feedback architecture. Therefore, the higher the output current amplitude, I, the higher the power, P, delivered to the device since $P = VI$. The frequency at which the measured current amplitude is maximized corresponds to the resonance frequency of the transducer. This feature effectively combats device-to-device differences and accounts for changes in circuit loading conditions, in particular the presence of liquid on the surface of the SAW or TM device. These factors often shift the resonance by 100 kHz or more, which is sufficient to significantly reduce the performance of an acoustic transducer, as most transducers have a quality factor * (Q) of >100, representing a very narrow bandwidth. Achieved by a straightforward electronics design and controlled by the MCU, this feature ensures all transducers are driven at their optimal frequency, despite any resonance changes. This might arise from the introduction of a new vial for drug atomization, too much fluid introduced in an experiment by accident, using the device at a different temperature, and so on.

The resonance search algorithm is verified against measurements from a vector network analyzer (VNA, E5071C Agilent Technologies, Inc., Santa Clara, CA USA) and a laser Doppler vibrometer (LDV, UHF-120SV, Polytec, Irvine, CA USA). A current spectrum resulting from a resonance search on the TM board reveals two peaks (Fig. 2(a)) from which the largest is chosen, thus identifying 6.62 MHz as the resonance of the transducer under test. The search is repeated with a drop of water on the transducer, which slightly shifts the resonance. Piezoelectric transducers can be modeled as a series combination of a frequency-dependent resistor, an inductor, and a capacitor. The impedance of such a circuit can be modeled as a complex function of frequency with a zero imaginary component at resonance, i.e., the inductive and capacitative components cancel out, leaving behind the real part: a pure resistance. This is equivalent to the frequency at which the S_{11} parameter, the input port voltage reflection coefficient from the VNA, intersects the real axis on a Smith chart (Fig. 2(b)). The closer the intercept point is to the origin, the lower the resistance, so the highest peak in Fig. 2(a) should occur at the same frequency as the left-most intercept in the Smith chart (Fig. 2(b)). Four thickness mode (TM) transducers intended for the TM board were all tested as shown in Fig. 2; each pair of frequencies identified with this technique agreed to within 0.2%. Similarly, a 40 MHz SAW transducer was tested and the VNA and the on-board algorithm were found to agree within 0.2% (Fig. 3). In each case, an LDV scan was performed over the region of interest on the transducer, and both the TM and SAW transducers were confirmed to have the largest amplitude at the frequency indicated by the on-board algorithm and the VNA.

2.3 Implementation in two examples

Here we elaborate on the circuit design for both the SAW board and the TM board. Details of their fabrication and assembly are provided in the Electronic Supplementary Information. The

* $Q = f_c/\Delta f$, where Q is the quality factor, f_c is the resonant frequency, and Δf is the width in frequency space of the corresponding peak at half the maximum amplitude. Quality factor is also intuitively associated with the energy loss of the oscillation [29].

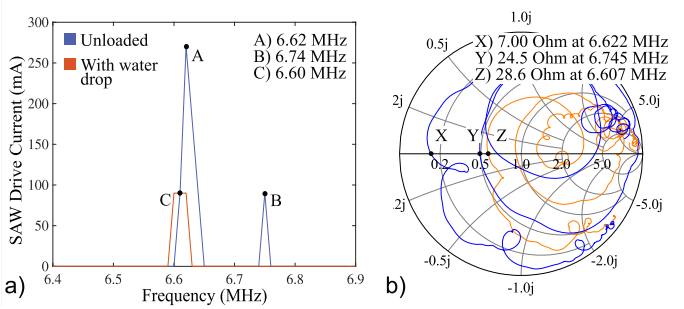

Fig. 2 A TM transducer was run through a frequency sweep using both the TM board and a VNA. Both a dry transducer (blue plots) and a transducer laden with a $\sim$5 $\mu\ell$ water drop (orange plots) were considered. (a) The current across the transducer is measured over the frequency range of interest by the MCU. A simple algorithm identifies the largest peak, in this case peak A when dry and peak C with water present. (b) Measured S_{11} of the TM transducer on a VNA. This confirms that the measured current peaks correspond to resonances of the transducer, both with and without liquid present. The messy appearance of the Smith chart is expected for a TM transducer with finite lateral dimensions, since spurious Lamb wave modes exist at similar frequencies. Despite this, the algorithm is still able to identify the desired TM mode for the drive circuit.

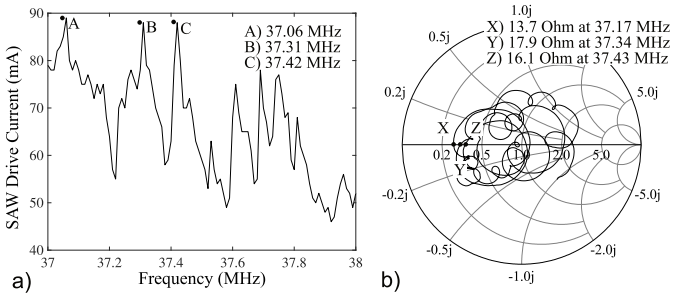

Fig. 3 A SAW IDT was run through a frequency sweep using both the SAW board and a VNA. (a) The current across the transducer is measured over the frequency range of interest by the MCU. The algorithm simply identifies the largest peak, in this case peak A. (b) Measured S_{11} of the SAW transducer on a VNA. This confirms that the measured current peaks correspond to resonances of the IDT. It is expected that multiple adjacent resonances—*side bands*—exist in an IDT that lacks specific design features, such as apodization, to prevent them.

thickness-mode (TM) board drives a 6–7 MHz thickness mode transducer to achieve a handheld nebulizer. SAW is impractical at less than 40 MHz because the penetration depth of the SAW is 4–5 wavelengths, exceeding the 500 μm thickness of the widely available piezoelectric lithium niobate wafers used for this purpose. The transducer is driven by 0.5 to 2 W of power. The SAW board has a similar design, but is tailored to drive a 40–120 MHz SAW device used to enhance the capacity of a rechargeable lithium metal battery. The SAW transducer typically demands 0.1 to 1 W of power in this application. The SAW devices demand as much as 5 W for atomization, the reason for the selection of other vibration modes that are more efficient in that application. However, the designs described here may be readily modified to produce driver circuits appropriate for these greater power requirements.

We will describe our choice of integrated circuits (ICs) for these applications. Since the TM board will be operated by a small 3.7 V battery, the power consumption of the electronics should be minimized. On the other hand, the SAW board operates at much higher frequencies, thus demanding higher-speed electronics. Fortunately, the board is powered by wall-wart supply, so the overall power consumption is of secondary concern. Note that the resulting boards, while fairly optimized, are not unique. Many IC options exist to accomplish the same function, each offering some trade-off in cost, size, performances, ease of assembly and usage. Engineers often start the design process by exploring and comparing ICs from the vast, searchable catalogues on electronic component distributors' web pages.

The SAW driver signal chain begins with the stimulus source. The complementary metal–oxide–semiconductor (CMOS) Si5351 (from Silicon Laboratories) clock generator (PLL) chip was employed to synthesize a tone with programmable frequency between 2.5 kHz to 300 MHz. It is followed by the CDCLVC1104 clock buffer (Texas Instruments, Dallas, TX USA). At 3.3 V input, it can operate up to 250 MHz. It is used to drive the attenuator that follows, preserve the low-skew clock, and accomplish duty-cycle control for pulse-width modulation. To shorten the development time, identical PLL and buffer circuits are used for both boards. Potential savings in cost and power did not warrant a customized design effort in this case.

Gain control is achieved by a programmable attenuator. The TM board features a "resistor divider" with a variable resistor (R2) achieved by an N-type metal-oxide-semiconductor (NMOS) transistor. Its resistance is digitally adjusted by the gate voltage fed by a voltage DAC (digital-to-analog converter) MCP4726 (from Microchip Technology). While this very simple implementation works well at low frequencies, the parasitic capacitance of the NMOS transistor will form a RC (R for resistance, C for capacitance) low-pass filter (LPF), distorting waveforms at higher frequencies. Therefore, the SAW board employs an active attenuator IC SKY12346 (from Skyworks Solutions). Designed for broadband cellular (up to 3 GHz) operation, the attenuator has no LPF or distortion issues, but at the expense of added direct current (DC) power consumption.

To boost the signal to drive the thickness mode device, the power amplifier section of the TM board employs one stage of a voltage feedback amplifier LM7171 (Texas Instruments). At 6.5 mA bias current, it features a unity-gain bandwidth of 200 MHz, sufficient to handle multiple harmonics of the clock to preserve the sharp, square waveform. On the other hand, the SAW board employs the amplifier THS3001 (also from TI), whose bandwidth reaches 420 MHz at slightly higher (10 mA) bias current. Moreover, gain is distributed into two stages. As the gain of each amplifier is lowered (halved), its stability at high frequencies, formally measured by the "phase margin", also improves. As the last stage of the signal chain, the power amplifier shall deliver high current to the SAW. To achieve that goal, a standard bipolar junction transistor (BJT) push-pull output driver is employed. Configured as emitter followers, a complementary PNP and NPN BJT pair (ECH8502, from ON semiconductor) can efficiently and rapidly pump and sink currents into and from the load.

The micro-controller (MCU) function is provided by the Arduino nano clone ATmega328P (from Microchip Technology) and the accompanying software. It is pre-loaded with programs to

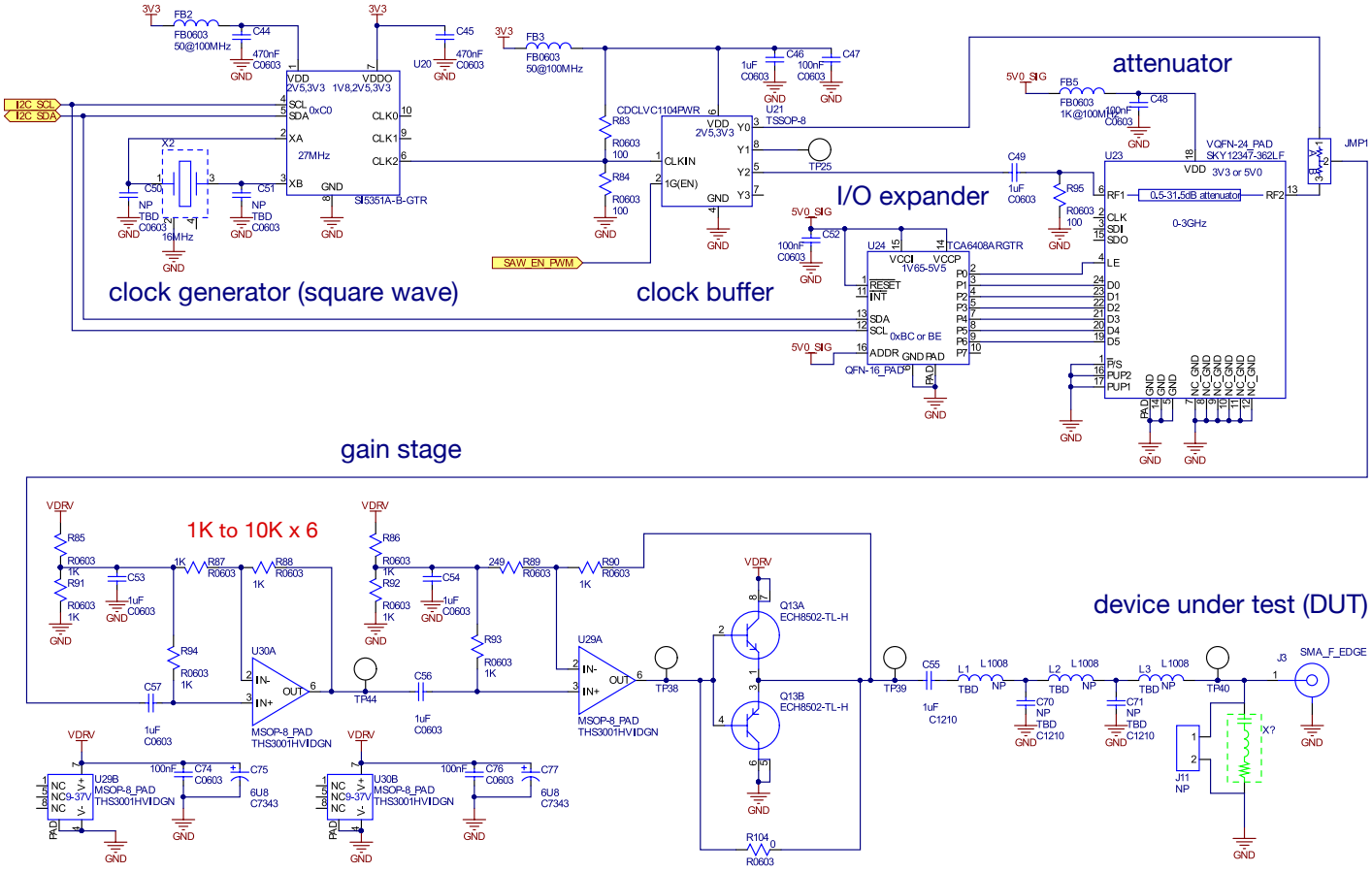

Fig. 4 Each circuit component is symbolically represented in this schematic organized for conceptual clarity.

calculate, based on user inputs and component parameters, the control signals for all ICs on the PCB. The input-output (I/O) expander chip TCA6408A (from Texas Instruments) provides eight bits of general-purpose parallel input/output expansion for the two-line bidirectional "I2C" bus protocol, simplifying all IC control and user interfaces.

For the power management unit (PMU), there are literally thousands of boost converter ICs (voltage step-up) and low-dropout (LDO) regulator ICs (voltage step-down) for designers to choose from, targeting different input/output voltage ranges and current ratings. The design process is fairly straightforward. For example, the main input of the TM board comes from a 3.7 V battery, and 3 V, 5 V and 24 V are desired. This is accomplished as follows: (1) a boost converter XCL101C (from Torex Semiconductor) steps up 3.7 V to generate 5 V; (2) an LDO regulator TLV733P (from Texas Instruments) steps down from 5 V to generate 3 V; and (3) a boost converter MP3213 (from Monolithic Power Systems) steps up from 3.7 V to 24 V. On the other hand, the main input of the SAW board comes from a 12 V wall wart supply, and 3.3 V, 5 V and 34 V are required. This is achieved by: (1) two LDO regulators MIC5225 (from Micrel Technology) stepping down 12 V to both 3.3 V and 5 V, and (2) a boost converter LT3489 (from Linear Technology) stepping up from 12 V to 34 V.

The current sensing function in the TM board is achieved by a 1Ω series resistor, directly performing current-to-voltage (I-to-V) conversion on the output sinusoidal current driving the SAW device. The corresponding voltage signal is subsequently amplified and rectified (LT1810, by Linear Technology); a diode (BA891, by NXP) provides peak detection from this signal. The resulting peak DC voltage is digitized by an ADC (analog-to-digital converter) embedded in the MCU. The MCU automatically sweeps the PLL (stimulus) frequencies over a pre-defined range and records all corresponding ADC values. Resonance is given by the frequency at which the peak ADC value occurs. The current sensing function in the SAW board is indirectly performed. High-frequency current signals vary too quickly for direct rectification and peak detection without disrupting the normal operation of the power amplifier. Instead, a current amplifier chip (LTC6101, by Analog Devices) is employed at the power supply of the driver amplifier.

2.4 Layout and testing

Having chosen the ICs and defined the circuit architecture, the design may be laid out on a custom-made printed circuit board (PCB). There are many commercially available computer-aided drafting (CAD) tools to aid with the PCB development process. Here, Altium Designer was employed. The design process begins by capturing all circuit components schematically (Fig. 4). Symbols representing ICs are connected to all required circuit components. The functions and performances of certain critical parts (e.g. the driver amplifiers) can be verified using circuit simulation

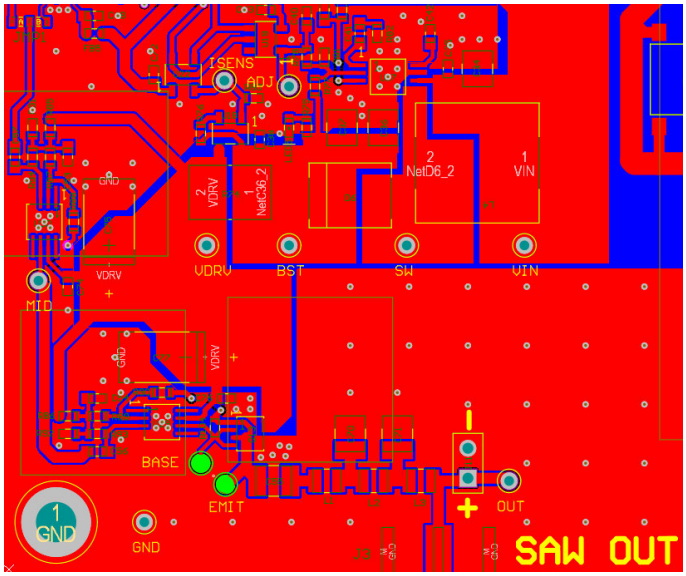

Fig. 5 The schematic in Fig. 4 is transformed into a PCB layout following a standard design procedure using a testing breadboard. This is sent out for fabrication and debugged before designing the final PCB layout with the desired form factor.

software such as LTspice®. All components are laid out according to design rules and manufacturing requirements while maintaining interconnectivity information generated by the schematic (Fig. 5). The completed PCB layout, together with the bill of materials, can then be submitted to commercial manufacturing companies for fabrication and assembly (i.e., electronic components and chips are populated and soldered onto the PCB). The finished PCB is then tested, debugged, and verified in the lab.

The above procedure entails a fair amount of design time, cost, and effort. In order to make the engineering tasks more manageable, especially when new chips or circuit functions were introduced, we adapt the following step-by-step approach. To start, we employ "evaluation boards" offered by chip vendors (e.g., Si535x–B20QFN–EVB for the phase-locked loop (PLL) from Silicon Labs) to test out the circuit functions rapidly. The drawback is the higher cost, and the clumsy interface and size. Next, we integrate all chips onto a relatively large, two-layer PCB, as shown in Fig. 5. Routings are done in a straight-forward manner, with all components mounted on only one side of the board, ICs with bigger packages are chosen for easier soldering and probing, and multiple test points and signal breaking points (with a 0ω resistor) are generously incorporated. To avoid signal noise, wide traces and large copper planes for ground and power are used. After this easy to build PCB has been debugged and the functionality verified, the layout is optimized to achieve the desired form factor. Board size is reduced by using double-sided, multilayer PCBs with dedicated ground and power planes. Testing features, with a few crucial exceptions, are removed. More densely packed components require more carefully planned routings to avoid long traces and signal cross-talk. The completed boards for the battery-powered TM device and mains-powered SAW device are depicted in Fig. 6 and Fig. 7, respectively, in nebulizer and particle alignment applications.

3 Application to handheld acoustofluidics devices

For microcircuit-driven acoustofluidic devices to be viable, they must perform similarly to benchtop devices designed and demonstrated in laboratories. We compare our handheld nebulizer—utilizing the TM board (Fig. 6(a)—with acoustofluidic atomization literature and with a benchtop driver setup with an identical transducer. The TM board has a custom program pre-loaded to facilitate use without further connection to a computer or other device. Such a pre-programmed board design is especially convenient in a prototype closer to use as a consumer product.

Similarly, we present three implementations of the SAW board and compare these results with benchtop-driven devices from the published literature and a benchtop signal generator and amplifier combination driving these same three devices in our own laboratory. The frequency, power, and duty cycle delivered by the SAW board can be selected by defining these parameters in a custom (MATLAB, Mathwords, Natick, MA USA) script uploaded from a connected PC to the board's MCU. An externally connected PC is required to change these settings with the SAW board, and the PC is convenient for real-time download of the operating state of the SAW board, making it possible to adjust the board's operation and detect the effects from the computer. This is much more difficult to accomplish with the pre-programmed TM board.

For consistency, during comparisons with benchtop setups, the same equipment is used in all four applications. Acoustic vibrations are produced by applying a sinusoidal voltage signal to the transducers using a signal generator (WF1967 multifunction generator, NF Corporation, Yokohama, Japan) and an amplifier (ZHL–1–2W–S+, Mini-Circuits, Brooklyn, NY USA). The instantaneous voltage and current are measured and used to compute the net power input via an oscilloscope (InfiniVision 2000 X-Series, Keysight Technologies, Santa Rosa, CA USA) as shown in Fig. 6(b).

3.1 Nebulization

Megahertz frequency acoustofluidic nebulization offers several advantages over current technology for delivering therapeutic proteins, cells, functionalized nanoparticles, and monoclonal antibodies to the lungs[19,30,31]. It is cheaper and less prone to clogging than the current state-of-the-art, ultrasonic mesh nebulizers. These operate at much lower frequencies and in order to generate droplets small enough for optimal lung delivery, and they must rely on 5 μm laser-cut holes in a metal plate through which a drug solution is forced[32,33]. Mesh nebulizers tend to be tailored to work with a particular solution and have a limited range of fluids that they will nebulize. Mesh nebulizers in general may cause damage to biomolecules due to high shear forces and kHz-order frequency operation[34,35]. By contrast, acoustofluidic nebulization has been demonstrated for delivery of antibodies[20,21] and DNA[19]. There is also some evidence—in unpublished work—that the droplet size can be adjustable during device operation. This could be necessary either between patients, for example adults and children, or in compensation for the changing airflow during

inhalation and exhalation. These aspects are important in seeking appropriate dose control in pulmonary delivery[19].

However, MHz-frequency nebulization is only competitive with mesh nebulizers if it can be decoupled from benchtop equipment, enabled for the first time with the TM board (Fig. 6). A previous attempt at such a circuit[36] did not provide sufficient power for consistent atomization, even with signal modulation intended to reduce the average power consumption[2]. Furthermore, this circuit could drive transducers at only a single, predetermined frequency, and had a short lifetime of a few hours.

We present a handheld nebulizer based on a lithium niobate TM transducer, which has been shown to produce higher efficiency atomization (flow rate per unit power input) than either SAW or other wave types in lithium niobate or TM in lead zirconate titanate (PZT)[37]. We drive the 3x10 mm TM lithium niobate transducers at their primary resonance frequency as indicated in Fig. 2, usually 6.6 MHz. The device consists of a transducer holder, a fluid supply system, and the TM board powered by a rechargeable lithium-ion battery (Fig. 6). The user interface consists of a power switch and five buttons: resonance frequency algorithm run, switch on or off, amplitude increase, amplitude decrease, and reset. The transducer holder provides electrical contact while minimizing mechanical damping of the acoustic waves. A video provided in the ESI † demonstrates operation of the nebulizer.

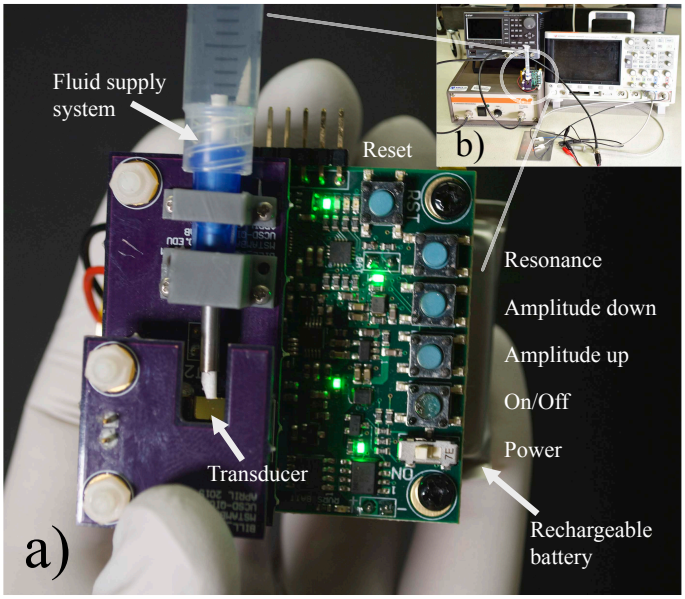

Fig. 6 (a) Major components of the handheld nebulizer are labeled along with the user interface. (b) Benchtop equipment—including signal generator, amplifier, oscilloscope, cables, and connections—typical of the acoustofluidic device experience—is entirely replaced by our small, inexpensive, and portable circuit.

Liquid is wicked from a reservoir through a fibrous nib onto the transducer surface. A physically hydrophilic region is ablated onto the surface of the transducer using an excimer laser (LaserShot, Optec, Belgium). This hydrophilic region and the capillary action of the nib help draw liquid out in a thin layer over the transducer. While the transducer is vibrating, acoustowetting provides additional flow forcing[38], leading to a semi-passive liquid supply system that ensures liquid is only drawn out during nebulization, which prevents flooding and drying out of the transducer surface. No active pumping mechanism is required.

We compare the performance of our 6.6 MHz handheld nebulizer to an equivalent atomization set-up with a benchtop signal generator and amplifier. The benchtop set-up can deliver greater power inputs and produces a pure sine wave voltage signal, which often produces a cleaner acoustic wave. The handheld device uses a square wave, which significantly reduces the complexity of the circuit, thus allowing it to fit in a smaller footprint and reducing development time and cost. More frequency modes are generally excited by a square wave, but we show that TM nebulization performance is unaffected. Figure 8(a) demonstrates that the droplet size distribution for water is not significantly affected by the voltage signal waveform. The maximum flow rate for a given power input, again, using water, is similar between the handheld and benchtop devices (Fig 8(b). These results are the same order of magnitude for maximum flow rate compared with the literature—Winkler *et al.* report 0.2 mℓ/min at 3.5 W for SAW[39] and Collignon *et al.* report 0.3 mℓ/min at 1.4 W for TM[37], all with water (though the latter does report a broader range of fluids). The majority of the atomized water volume occurs in droplets less than 10 μm, ideal for pulmonary drug delivery. The power output of the handheld device is currently limited by a maximum voltage of 22 V (equivalent to $\sim$2 W in this case), which is sufficient for all but the most demanding acoustofluidics applications. It may be increased, but such an increase must be balanced against the cost and time of further development and any size or battery constraints.

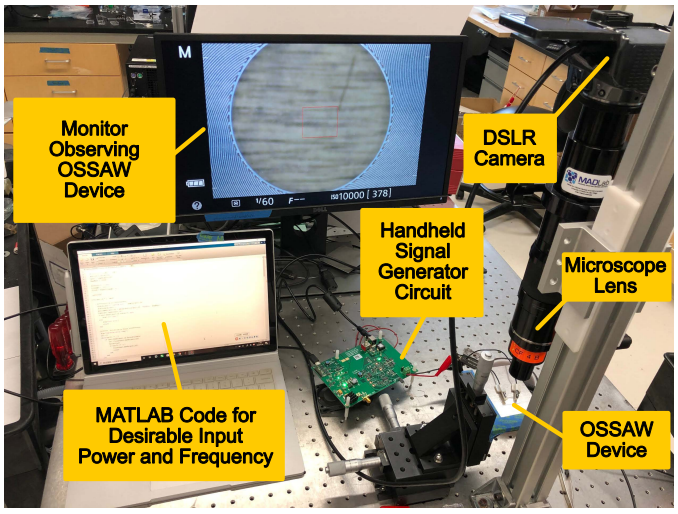

Fig. 7 An example of the SAW board in use for SAW-induced particle separation.

SAW board set up

Here we provide a sample image of the SAW board during its use to perform a typical acoustofluidics-based chip operation. Please also consult the video provided in the ESI † that demonstrates operation of the SAW board during fluid mixing.

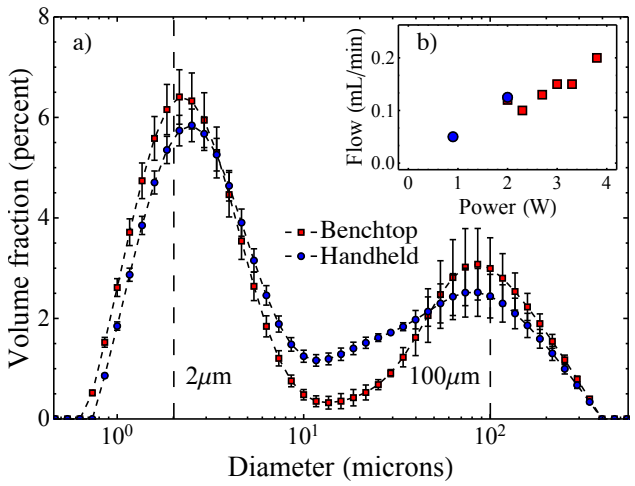

Fig. 8 (a) Droplet size distributions were obtained using a laser diffraction particle sizer (Spraytec, Malvern). Three measurements were taken for both the benchtop set-up and the handheld device and the mean values and standard errors are reported. Identical electrical/mechanical contact and fluid supply was used in each case and in each case the transducer was driven at 6.6 MHz and 2 W. Notice that the distribution is in terms of volume fraction so that a small number of large droplets produces a relatively large peak—the vast majority of droplets are close to 2 μm. (b) For experiments in this plot alone, for the purpose of accuracy, flow rates were imposed using a syringe pump. The power was adjusted until atomization was sustainable—no sputtering and no flooding. Again the transducer contact and fluid supply were identical in both the benchtop set-up and the handheld device.

3.2 Mixing in liquid droplets

Rapid and complete mixing in microfludics and nanofludics is needed in time-sensitive chemical reactions and bio-chemical processes[6,40]. However, diffusion dominates micro scale mixing because the flow is usually laminar. Such diffusion-based mixing is too slow for most lab-on-a-chip applications especially for biological samples. Adopting surface acoustic wave (SAW) induced acoustic streaming to generate chaotic advection is a solution to increase the diffusion rate and decrease the mixing time significantly, as shown by Shilton et al.[41].

We illustrate rapid mixing in a simple experimental setup. A single droplet contains two initially separate liquids—a 1 $\mu\ell$ transparent glycerol drop is first placed on the surface and then a 0.25 $\mu\ell$ blue-color dyed water drop is placed into the glycerol droplet (*see* Fig. 9(a)). A 40 MHz SAW device is chosen to produce efficient mixing between the two droplets. Fig. 9(b) shows a drop that has been mixed using benchtop equipment for 7 s at 280 mW. Fig. 9(c) shows a drop that has been mixed for 6 s at 300 mW using a handheld circuit as illustrated in Fig. 7. These results are essentially equivalent and are on par with literature values, for example, Shilton *et al.* report complete mixing of colored dye into a glycerol solution in 8 s at ∼1 W (the excess power is because there was a microfluidic well instead of a sessile drop in that case, which increases attenuation).

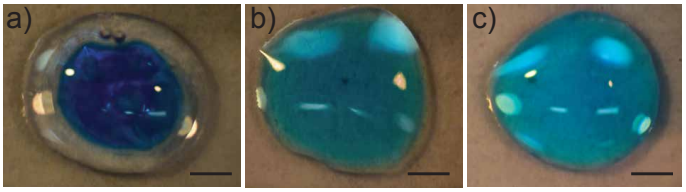

Fig. 9 Effective droplet mixing via travelling surface acoustic wave. The water droplet is dyed with blue color (the middle ring), while the glycerol droplet remains transparent. (a) is the pre-mixing stage, (b) and (c) are the post-mixing stage via external driven power caused chaotic mixing with benchtop signal generator with power amplifier and handheld circuit boards, respectively. The scale bar represents 250 μm.

3.3 Microparticle separation within a microliter sessile droplet

Particle and cell separation induced by SAW in sessile drops has become a popular platform due to its convenience, rapid response, and biocompatibility. Straight and standard interdigital transducers (IDTs) with a sessile drop located at an offset position from the center of the SAW propagation direction have been used to spin fluid droplets, producing particle concentration and separation due to asymmetric SAW actuation[9,42,43]. We have recently produced a novel omnidirectional spiral surface acoustic wave (OSSAW) interdigital transducer design. This spiral design was developed such that the wave propagation direction is always rotationally symmetric and tangent to a circle inside the IDT structure (*see* Fig. 10). This allows the production of inward-bound acoustic waves ideal to spin a droplet, but only because we have placed the IDT on a selected cut of lithium niobate that allows the production of SAW in any direction[44]. We further demonstrated accurate particle manipulation and multi-size separation in a microliter ($\mu\ell$) drop with this effort.

Here, we perform microparticle separation with the same OSSAW transducer, but now employ the SAW board instead of a standard benchtop setup. An operating frequency of 40 MHz was chosen to produce a ∼8 μm particle/cell separation threshold, taking into account particle compressibility[45–47]. Polystyrene (PS) particles (Polysciences, Inc., Warrington, PA, USA) with diameters of 4 and 38 μm were selected to show size-selective separation at the microscale. A 1 $\mu\ell$ droplet containing these particles in concentrations of 4×10^9 and 1×10^5 particles/mℓ, respectively, was placed at the center of the transducer. After ∼5 s at ∼1 W, the smaller particles collected at the periphery and the larger particles concentrated at the center (*see* Fig. 11b-d and a video in the ESI †). The same result was obtained with either the SAW board or the benchtop equipment described above and it is reasonably comparable to past work[42] using lab equipment, where 6 μm and 31 μm particles were separated using 20 MHz SAW at 250 mW in ∼4 s. Our implementation requires more power for a similarly sized sessile drop because the frequency is much higher, which causes greater attenuation but produces superior separation selectivity based on particle size.

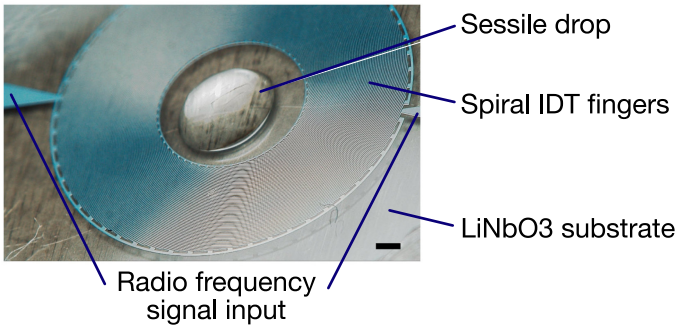

Fig. 10 A 60-MHz OSSAW device with a microliter sessile drop in the inner circular region, showing the fingers and electrode connection to produce a suitable spiral SAW. Scale bar: 0.5 mm.

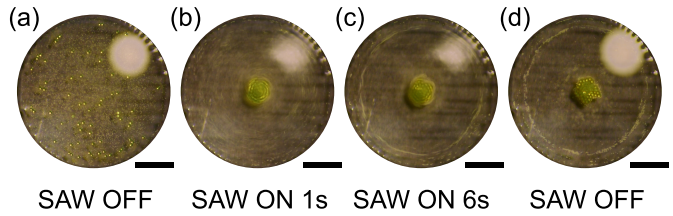

Fig. 11 Effective particle separation via omnidirectional spiral surface acoustic waves (OSSAW) with size of 38 μm and 4 μm operated at a resonance frequency of 40 MHz. (a) Before SAW actuation, (b) 1 s after SAW is on, (c) 6 s after SAW is on, and (d) after SAW actuation. Scale bar: 0.5 mm. The bright dot at the top right of the droplet is the light reflection from the droplet boundary.

3.4 Particle alignment

Particle alignment via collection at nodes of acoustic standing waves has been demonstrated for applications such as tissue engineering[48] and cell characterization[10] and serves as a fundamental tool wherever small particles need to be patterned. Utilizing acoustic forces rather than laser actuation as in optical tweezers prevents damage to cells and does not rely on the magnetic or electric properties of the particles. Standing waves generated by counter propagating SAWs with the same frequency create stationary pressure nodes, where suspended particles can be trapped by acoustic radiation force. The spacing between adjacent nodes is determined by the wavelength ($\lambda/2$). Chirped IDTs allow for a range of frequencies to be used in the same transducer so that the nodal and anti-nodal positions can be changed at will[17,49].

We present particle alignment and patterning with adjustable spacing driven by the SAW board. Two pairs of chirped IDTs with resonance frequencies in the range 40–80 MHz were fabricated around a 6 mm by 6 mm closed glass chamber 100 μm in height (*see* Fig. 12). Fluorescent polymer particles 2.1 μm in diameter were aligned in various patterns based on the signals generated with the SAW board. When only one pair of IDTs, as shown in Fig. 13(a) and (b), are powered at 40.2 MHz, the particles are aligned in lines with 48.5 μm separation, close to one half the SAW wavelength (49.9 μm); this wavelength is the relevant one as the particles are near the substrate[50]. When all four IDTs are actuated, particles assemble around nodal points to form an equally spaced array. With the chirped IDT, the spacing may be adjusted by changing the frequency. Fig. 13(c), (d) and (e) display the arrays at 40.2 MHz, 59.8 MHz and 79.4 MHz, respectively, resulting in 48.3 μm, 34.1 μm and 25.3 μm spacing. A comparison of results obtained with the SAW board and with the benchtop equipment are given in Table 1, which shows nearly identical results. This capability closely mimics that demonstrated by Shi *et al.* where 2 μm particles were aligned to a grid with $\sim$50 μm spacing in a matter of seconds[51].

Table 1 Comparison of handheld device and regular signal generator.

	Handheld device	Signal generator
Frequency (MHz)	40.2	40.2
Voltage output	70%	1.69 V
Oscilloscope read	2.1 V	2.1 V
Response time	7.0 s	6.8 s
Spacing (μm)	48.3	49.1

4 Conclusions

Acoustofluidics devices have—for far too long—betrayed the ideal of "lab-on-a-chip", bringing instead to mind the tired old joke "chip-in-a-lab" from all the signal generation and monitoring

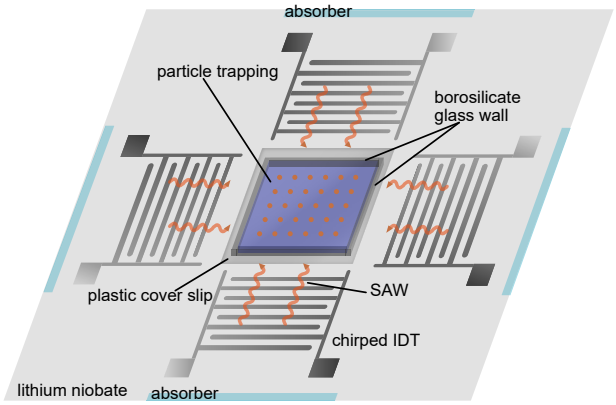

Fig. 12 A schematic of the 2D alignment device. Four-way chirped IDTs create a series of regular pressure nodes where particles are entrapped.

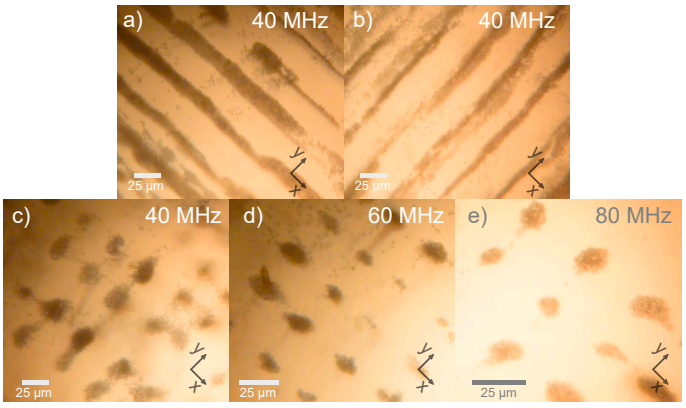

Fig. 13 When only two IDTs are actuated, particles are aligned in lines along (a) the x direction or (b) the y direction depending on which pair of IDTs are actuated (in this case at 40.2 MHz). When 4 IDTs are actuated at the same time, particles are aligned in an array with different separations at corresponding frequencies: (c) 40 MHz, (d) 60 MHz and (e) 80 MHz. Scale bar: 25 μm.

equipment tethering the devices to a lab bench just to get them to function. No longer. Acoustofluidics may now be used in practical lab-on-a-chip and point-of-care devices with the circuit design information and simple examples provided in this paper. Our aim in this contribution is to enable those trained merely in the basics of electrical circuits to be able to devise and fabricate a design for their needs. Our approach is suitable for providing controlled signals to drive 1–300 MHz acoustic devices from 50 mW to 2 W of power and, with some work by the reader, these ranges may be greatly expanded while maintaining either the mains or battery-powered, handheld format needed in many applications. Using the design principles espoused in Section 2, we have demonstrated a completely handheld, battery-powered acoustic device driver (the TM board) for a high-power application: atomization. We have also demonstrated a mains-powered design (the SAW board) with a computer interface useful for monitoring and controlling the operation of the driver circuit, including the power and frequency of the signal supplied to the acoustic device. This design was used for acoustic devices to produce liquid mixing, particle separation, and particle alignment exemplifying many of the operations needed in micro to nano-scale fluidics devices.

During these tests, these driver boards delivered signals equivalent to the much larger benchtop or rack-mount laboratory signal generation, amplification, and monitoring equipment in use in many researchers' laboratories. Crucially, these driver boards *also* offer resonance tracking, power management, and signal monitoring features absent in laboratory equipment and necessary in the unpredictable clinical and industrial environments where these devices will be used. Together, these implementations show how almost any embodiment of acoustofluidic research could be miniaturized and rendered conveniently portable.

Conflicts of interest

The authors declare no conflicts of interest.

Acknowledgements

The authors are grateful to the University of California, the Qualcomm Institute, and the NANO3 facility at UC San Diego for provision of funds and facilities in support of this work. This work was performed in part at the San Diego Nanotechnology Infrastructure (SDNI) of UCSD, a member of the National Nanotechnology Coordinated Infrastructure, which is supported by the National Science Foundation (Grant ECCS—1542148). The work presented here was generously supported by a research grant to J. Friend from the W.M. Keck Foundation. He is furthermore grateful for the support of this work by the Office of Naval Research (via grants 12368098 and N00014–20–P–2007), the Department of Energy via grant DE–EE0008363, and Kratos Defense via gift R–86X16–VX16.

Notes and references

1 A. Wixforth, *Superlattices and Microstructures*, 2003, **33**, 389–396.

2 A. Rajapaksa, A. Qi, L. Y. Yeo, R. Coppel and J. R. Friend, *Lab on a Chip*, 2014, **14**, 1858–1865.

3 H. Bachman *et al.*, *Lab on a Chip*, 2018, **18**, 433–441.

4 H. Bachman, H. Fu, P.-H. Huang, Z. Tian, J. Embry-Seckler, J. Rufo, Z. Xie, J. H. Hartman, S. Zhao, S. Yang *et al.*, *Lab on a Chip*, 2019, **19**, 2404–2414.

5 X. Ding, P. Li, S.-C. S. Lin, Z. S. Stratton, N. Nama, F. Guo, D. Slotcavage, X. Mao, J. Shi, F. Costanzo *et al.*, *Lab on a Chip*, 2013, **13**, 3626–3649.

6 J. R. Friend and L. Y. Yeo, *Reviews of Modern Physics*, 2011, **83**, 647–704.

7 W. Connacher, N. Zhang, A. Huang, J. Mei, S. Zhang, T. Gopesh and J. Friend, *Lab on a Chip*, 2018, **18**, 1952–1996.

8 H. Li, J. Friend, L. Yeo, A. Dasvarma and K. Traianedes, *Biomicrofluidics*, 2009, **3**, 034102.

9 H. Li, J. R. Friend and L. Y. Yeo, *Biomedical Microdevices*, 2007, **9**, 647–656.

10 Y. Chen, S. Li, Y. Gu, P. Li, X. Ding, L. Wang, J. P. McCoy, S. J. Levine and T. J. Huang, *Lab on a Chip*, 2014, **14**, 924–930.

11 M. N. Topp, *Journal of Aerosol Science*, 1973, **4**, 17–25.

12 T. Frommelt, M. Kostur, M. Wenzel-Schäfer, P. Talkner, P. Hänggi and A. Wixforth, *Physical Review Letters*, 2008, **100**, 034502.

13 K. Sritharan, C. Strobl, M. Schneider, A. Wixforth and Z. v. Guttenberg, *Applied Physics Letters*, 2006, **88**, 054102.

14 R. Shilton, M. K. Tan, L. Y. Yeo and J. R. Friend, *Journal of Applied Physics*, 2008, **104**, 014910.

15 S. Meyer dos Santos, A. Zorn, Z. Guttenberg, B. Picard-Willems, C. Kläffling, K. Nelson, U. Klinkhardt and S. Harder, *Biomicrofluidics*, 2013, **7**, 056502.

16 L. Tian, N. Martin, P. G. Bassindale, A. J. Patil, M. Li, A. Barnes, B. W. Drinkwater and S. Mann, *Nature communications*, 2016, **7**, 1–10.

17 X. Ding, S.-C. S. Lin, B. Kiraly, H. Yue, S. Li, I.-K. Chiang, J. Shi, S. J. Benkovic and T. J. Huang, *Proceedings of the National Academy of Sciences*, 2012, **109**, 11105–11109.

18 M. Wu, Y. Ouyang, Z. Wang, R. Zhang, P.-H. Huang, C. Chen, H. Li, P. Li, D. Quinn, M. Dao *et al.*, *Proceedings of the National Academy of Sciences*, 2017, **114**, 10584–10589.

19 A. E. Rajapaksa, J. J. Ho, A. Qi, R. Bischof, T.-H. Nguyen, M. Tate, D. Piedrafita, M. P. McIntosh, L. Y. Yeo, E. Meeusen *et al.*, *Respiratory Research*, 2014, **15**, 60.

20 C. Cortez-Jugo, A. Qi, A. Rajapaksa, J. R. Friend and L. Y. Yeo, *Biomicrofluidics*, 2015, **9**, 052603.

21 A. E. Rajapaksa, L. A. H. Do, D. Suryawijaya Ong, M. Sourial, D. Veysey, R. Beare, W. Hughes, W. Yang, R. J. Bischof, A. McDonnell *et al.*, *Frontiers in Pharmacology*, 2020, **11**, 1291.

22 M. B. Dentry, L. Y. Yeo and J. R. Friend, *Physical Review E*, 2014, **89**, 013203.

23 A. Ozcelik, J. Rufo, F. Guo, Y. Gu, P. Li, J. Lata and T. J. Huang, *Nature Methods*, 2018, **15**, 1021–1028.

24 G. Destgeer and H. J. Sung, *Lab on a Chip*, 2015, **15**, 2722–2738.

25 A. Huang, H. Liu, O. Manor, P. Liu and J. Friend, *Advanced Materials*, 2020, **32**, 1907516.

26 A. Winkler, R. Brünig, C. Faust, R. Weser and H. Schmidt, *Sensors and Actuators A: Physical*, 2016, **247**, 259–268.

27 M. G. Kim, S. Yoon, H. H. Kim and K. K. Shung, *Ultrasonics*, 2016, **65**, 258–267.

28 V. T. Rathod, *Electronics*, 2019, **8**, 169.

29 C. K. Campbell, *Proceedings of the IEEE*, 1989, **77**, 1453–1484.

30 M. Alvarez, J. Friend and L. Y. Yeo, *Nanotechnology*, 2008, **19**, 455103.

31 A. Qi, L. Yeo, J. Friend and J. Ho, *Lab on a Chip*, 2010, **10**, 470–476.

32 J. Waldrep and R. Dhand, *Current Drug Delivery*, 2008, **5**, 114–119.

33 K. H. Chang, S.-H. Moon, J. Y. Oh, Y.-S. Yoon, N. Gu, C.-Y. Lim, B. J. Park and K. C. Nam, *Pharmaceutics*, 2019, **11**, 192.

34 A. Aver'yanov, A. Konoplyannikov, N. Antonov, G. Osipova, O. Vasil'eva, M. Sakharova, A. Tatarskii and V. Kobylyansky, *Bulletin of Experimental Biology and Medicine*, 2018, **164**, 576–578.

35 A. Astudillo, S. S. Y. Leung, E. Kutter, S. Morales and H.-K. Chan, *European Journal of Pharmaceutics and Biopharmaceutics*, 2018, **125**, 124–130.

36 A. Qi, J. R. Friend, L. Y. Yeo, D. A. Morton, M. P. McIntosh and L. Spiccia, *Lab on a Chip*, 2009, **9**, 2184–2193.

37 S. Collignon, O. Manor and J. Friend, *Advanced Functional Materials*, 2018, **28**, 1704359.

38 G. Altshuler and O. Manor, *Physics of Fluids*, 2015, **27**, 102103.

39 A. Winkler, S. Harazim, D. Collins, R. Brünig, H. Schmidt and S. Menzel, *Biomedical Microdevices*, 2017, **19**, 9.

40 G. Whitesides, *Lab on a Chip*, 2014, **14**, 3125–3126.

41 R. J. Shilton, L. Y. Yeo and J. R. Friend, *Sensors and Actuators B: Chemical*, 2011, **160**, 1565–1572.

42 P. R. Rogers, J. R. Friend and L. Y. Yeo, *Lab on a Chip*, 2010, **10**, 2979–2985.

43 G. Destgeer, H. Cho, B. H. Ha, J. H. Jung, J. Park and H. J. Sung, *Lab on a Chip*, 2016, **16**, 660–667.

44 N. Zhang, J. Mei, T. Gopesh and J. Friend, *IEEE Transactions on Ultrasonics, Ferroelectrics, and Frequency Control*, 2020, 2176–2186.

45 L. V. King *et al.*, *Proc. R. Soc. Lond. A*, 1934, **147**, 212–240.

46 A. Doinikov, *Proceedings of the Royal Society of London. Series A: Mathematical and Physical Sciences*, 1994, **447**, 447–466.

47 F. Nadal and E. Lauga, *Physics of Fluids*, 2014, **26**, 082001.

48 J. P. Lata, F. Guo, J. Guo, P.-H. Huang, J. Yang and T. J. Huang, *Advanced Materials*, 2016, **28**, 8632–8638.

49 K. Chen, M. Wu, F. Guo, P. Li, C. Y. Chan, Z. Mao, S. Li, L. Ren, R. Zhang and T. J. Huang, *Lab on a Chip*, 2016, **16**, 2636–2643.

50 O. Manor, L. Y. Yeo and J. R. Friend, *Journal of Fluid Mechan-*

ics, 2012, **707**, 482–495.

51 J. Shi, D. Ahmed, X. Mao, S.-C. S. Lin, A. Lawit and T. J. Huang, *Lab on a Chip*, 2009, **9**, 2890–2895.